Batch Normalization is a Cause of Adversarial Vulnerability

Angus Galloway [1 2] **Anna Golubeva** [3 4 2] **Thomas Tanay** [5] **Medhat Moussa** [1] **Graham Taylor** [1 2 6]

Abstract

Batch normalization (batch norm) is often used in an attempt to stabilize and accelerate training in deep neural networks. In many cases it indeed decreases the number of parameter updates required to achieve low training error. However, it also reduces robustness to small adversarial input perturbations and noise by double-digit percentages, as we show on five standard datasets. Furthermore, substituting weight decay for batch norm is sufficient to nullify the relationship between adversarial vulnerability and the input dimension. Our work is consistent with a mean-field analysis that found that batch norm causes exploding gradients.

1. Introduction

Batch norm is a standard component of modern deep neural networks, and tends to make the training process less sensitive to the choice of hyperparameters in many cases (Ioffe & Szegedy, 2015). While ease of training is desirable for model developers, an important concern among stakeholders is that of model robustness to plausible, previously unseen inputs during deployment.

The adversarial examples phenomenon has exposed unstable predictions across state-of-the-art models (Szegedy et al., 2014). This has led to a variety of methods that aim to improve robustness, but doing so effectively remains a challenge (Athalye et al., 2018; Schott et al., 2019; Hendrycks & Dietterich, 2019; Jacobsen et al., 2019). We believe that a prerequisite to developing methods that increase robustness is an understanding of factors that reduce it.

Approaches for improving robustness often begin with existing neural network architectures—that use batch norm—and patching them against specific attacks, e.g., through inclusion of adversarial examples during training (Szegedy et al., 2014; Goodfellow et al., 2015; Kurakin et al., 2017; Mądry et al., 2018). An implicit assumption is that batch norm itself does not reduce robustness – an assumption that we tested empirically and found to be invalid. In the original work that introduced batch norm, it was suggested that other forms of regularization can be turned down or disabled when using it without decreasing standard test accuracy. Robustness, however, is less forgiving: it is strongly impacted by the disparate mechanisms of various regularizers.

The frequently made observation that adversarial vulnerability can scale with the input dimension (Goodfellow et al., 2015; Gilmer et al., 2018; Simon-Gabriel et al., 2018) highlights the importance of identifying regularizers as more than merely a way to improve test accuracy. In particular, batch norm was a confounding factor in Simon-Gabriel et al. (2018), making the results of their initialization-time analysis hold after training. By adding ℓ_2 regularization and removing batch norm, we show that there is no *inherent* relationship between adversarial vulnerability and the input dimension.

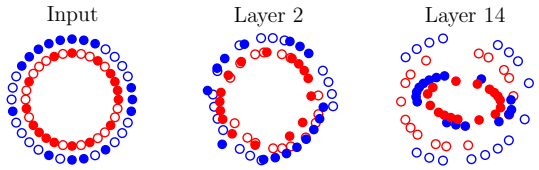

Figure 1. Two mini-batches from the "Adversarial Spheres" dataset (2D), and their representations in a deep linear network with batch norm at initialization. Mini-batch membership is indicated by marker fill and class membership by colour. Each layer is projected to its two principal components. Classes are mixed by Layer 14.

2. Batch Normalization

We briefly review how batch norm modifies the hidden layers' pre-activations h of a neural network. We use the notation of Yang et al. (2019), where α is the index for a neuron, l for the layer, and i for a mini-batch of B samples

[1]School of Engineering, University of Guelph [2]Vector Institute for Artificial Intelligence [3]Department of Physics and Astronomy, University of Waterloo [4]Perimeter Institute for Theoretical Physics [5]Huawei Noah's Ark Lab (work done while at University College London) [6]Google Brain. Correspondence to: Angus Galloway, Graham Taylor <gallowaa, gwtaylor@uoguelph.ca>.

Presented at the ICML 2019 Workshop on Identifying and Understanding Deep Learning Phenomena.

from the dataset; N_l denotes the number of neurons in layer l, W^l is the matrix of weights and b^l is the vector of biases that parametrize layer l. The batch mean is defined as $\mu_\alpha = \frac{1}{B}\sum_i h_{\alpha i}$, and the variance is $\sigma_\alpha^2 = \frac{1}{B}\sum_i (h_{\alpha i} - \mu_\alpha)^2$. In the batch norm procedure, the mean μ_α is subtracted from the pre-activation of each unit $h^l_{\alpha i}$ (consistent with Ioffe & Szegedy (2015)), the result is divided by the standard deviation σ_α plus a small constant c to prevent division by zero, then scaled and shifted by the learned parameters γ_α and β_α, respectively. This is described in Eq. (1), where a per-unit nonlinearity ϕ, e.g., ReLU, is applied after the normalization.

$$h_i^l = W^l \phi(\tilde{h}_i^{l-1}) + b^l, \qquad \tilde{h}^l_{\alpha i} = \gamma_\alpha \frac{h_{\alpha i} - \mu_\alpha}{\sqrt{\sigma_\alpha^2 + c}} + \beta_\alpha \quad (1)$$

Note that this procedure fixes the first and second moments of all neurons α equally at initialization. This suppresses the information contained in these moments. Because batch norm induces a non-local batch-wise nonlinearity to each unit α, this loss of information cannot be recovered by the parameters γ_α and β_α.

To understand how batch normalization is harmful, consider two mini-batches that differ by only a *single* example: due to the induced batch-wise nonlinearity, they will have different representations for *each* example (Yang et al., 2019). This difference is further amplified by stacking batch norm layers. Conversely, batch normalization of intermediate representations for two different inputs impair the ability to distinguish high-quality examples (as judged by an "oracle") that ought to be classified with a large prediction margin, from low-quality, i.e., more ambiguous, instances.

We argue that this information loss and inability to maintain relative distances in the input space reduces adversarial as well as general robustness. Figure 1 shows a degradation of class-relevant input distances in a batch-normalized linear network on a 2D variant of the "Adversarial Spheres" dataset (Gilmer et al., 2018).[1]

3. Empirical Result

We first evaluate the robustness (quantified as the drop in test accuracy under input perturbations) of convolutional networks, with and without batch norm, that were trained using standard procedures. The datasets – MNIST, SVHN, CIFAR-10, and ImageNet – were normalized to zero mean and unit variance.

As a white-box adversarial attack we use projected gradient descent (PGD), ℓ_∞- and ℓ_2-norm variants, for its simplicity and ability to degrade performance with little perceptible change to the input (Mądry et al., 2018). We run PGD for 20 iterations, with $\epsilon_\infty = 0.03$ and a step size of $\epsilon_\infty/10$ for SVHN, CIFAR-10, and $\epsilon_\infty = 0.01$ for ImageNet. For PGD-ℓ_2 we set $\epsilon_2 = \epsilon_\infty\sqrt{d}$, where d is the input dimension. We report the test accuracy for additive Gaussian noise of zero mean and variance $1/4$, denoted as "Noise" (Ford et al., 2019), as well as the full CIFAR-10-C common corruption benchmark (Hendrycks & Dietterich, 2019) in Appendix C.

We found these methods were sufficient to demonstrate a considerable disparity in robustness due to batch norm, but this is not intended as a formal security evaluation. All uncertainties are the standard error of the mean.[2]

For the SVHN dataset, models were trained by stochastic gradient descent (SGD) with momentum 0.9 for 50 epochs, with a batch size of 128 and initial learning rate of 0.01, which was dropped by a factor of ten at epochs 25 and 40. Trials were repeated over five random seeds. We show the results of this experiment in Table 1, finding that despite batch norm increasing clean test accuracy by $1.86 \pm 0.05\%$, it reduced test accuracy for additive noise by $5.5 \pm 0.6\%$, for PGD-ℓ_∞ by $17 \pm 1\%$, and for PGD-ℓ_2 by $20 \pm 1\%$.

Table 1. Test accuracies of VGG8 on SVHN.

BN	Clean	Noise	PGD-ℓ_∞	PGD-ℓ_2
✗	92.60 ± 0.04	83.6 ± 0.2	27.1 ± 0.3	22.0 ± 0.8
✓	94.46 ± 0.02	78.1 ± 0.6	10 ± 1	1.6 ± 0.3

For the CIFAR-10 experiments we trained models with a similar procedure as for SVHN, but with random 32×32 crops using four-pixel padding, and horizontal flips.

In the first experiment, a basic comparison with and without batch norm shown in Table 2, we evaluated the best model in terms of test accuracy after training for 150 epochs with a fixed learning rate of 0.01. In this case, inclusion of batch norm reduces the clean generalization gap (difference between training and test accuracy) by $1.1 \pm 0.2\%$. For additive noise, test accuracy drops by $6 \pm 1\%$, and for PGD perturbations by $17.3 \pm 0.7\%$ and $5.9 \pm 0.4\%$ for ℓ_∞ and ℓ_2 variants, respectively. Very similar results, presented in Table 3, are obtained on a new test set, CIFAR-10.1 v6 (Recht et al., 2018): batch norm slightly improves the clean test accuracy (by $2.0 \pm 0.3\%$), but leads to a considerable drop in test accuracy for the cases with additive noise and the two

Table 2. Test accuracies of VGG8 on CIFAR-10.

BN	Clean	Noise	PGD-ℓ_∞	PGD-ℓ_2
✗	87.9 ± 0.1	78.9 ± 0.6	52.9 ± 0.6	65.6 ± 0.3
✓	88.7 ± 0.1	73 ± 1	35.7 ± 0.3	59.7 ± 0.3

[1] We add a ReLU nonlinearity when attempting to *learn* the binary classification task posed by Gilmer et al. (2018) in Appendix D, but the activations in the linear case give us pause.

[2] Each experiment has a unique uncertainty, hence the number of decimal places varies.

Table 3. Test accuracies of VGG8 on CIFAR-10.1 (`v6`).

BN	Clean	Noise	PGD-ℓ_∞	PGD-ℓ_2
✗	75.3 ± 0.2	66 ± 1	36 ± 1	53.4 ± 0.5
✓	77.3 ± 0.2	60 ± 2	21.1 ± 0.8	49.9 ± 0.2

Table 4. VGG models of increasing depth on CIFAR-10, with and without batch norm (BN). See text for differences in hyperparameters compared to Table 2.

Model		Test Accuracy (%)		
L	BN	Clean	Noise	PGD-ℓ_∞
8	✗	89.29 ± 0.09	81.7 ± 0.3	55.6 ± 0.4
8	✓	90.49 ± 0.01	77 ± 1	40.6 ± 0.6
11	✗	90.4 ± 0.1	81.5 ± 0.5	53.7 ± 0.2
11	✓	91.19 ± 0.06	79.3 ± 0.6	43.8 ± 0.5
13	✗	91.74 ± 0.02	77.8 ± 0.7	40.3 ± 0.7
13	✓	93.0 ± 0.1	67 ± 1	28.5 ± 0.4
16	✓	92.8 ± 0.1	66 ± 2	28.9 ± 0.2
19	✓	92.65 ± 0.09	68 ± 2	30.0 ± 0.1

PGD variants.

It has been suggested that one of the benefits of batch norm is that it facilitates training with a larger learning rate (Ioffe & Szegedy, 2015; Bjorck et al., 2018). We test this from a robustness perspective in an experiment summarized in Table 4, where the initial learning rate was increased to 0.1 when batch norm was used. We prolonged training for up to 350 epochs, and dropped the learning rate by a factor of ten at epoch 150 and 250 in both cases, which increases clean test accuracy relative to Table 2. The deepest model that was trainable using standard He et al. (2015) initialization without batch norm was VGG13. [3] None of the deeper models with batch norm recover the robustness of the most shallow, or same-depth equivalents without batch norm, nor does the higher learning rate in conjunction with batch norm improve robustness compared to baselines trained for the same number of epochs. Additional results for deeper models on SVHN and CIFAR-10 can be found in Appendix A.

We evaluated the robustness of pre-trained ImageNet models from the `torchvision.models` repository.[4] Results are shown in Table 5, where batch norm improves top-5 accuracy on noise in some cases, but consistently reduces it by 8.54% to 11.00% (absolute) for PGD. The trends are the same for top-1 accuracy, only the absolute values were smaller; the degradation varies from 2.38% to 4.17%. Given the discrepancy between noise and PGD for ImageNet, we conduct a black-box transfer analysis in Appendix A.4.

Table 5. Models from `torchvision.models` pre-trained on ImageNet, some with and some without batch norm (BN).

Model		Top 5 Test Accuracy (%)		
Model	BN	Clean	Noise	PGD-ℓ_∞
VGG-11	✗	88.63	49.16	37.12
VGG-11	✓	89.81	49.95	26.12
VGG-13	✗	89.25	52.55	29.16
VGG-13	✓	90.37	52.12	20.63
VGG-16	✗	90.38	60.67	32.81
VGG-16	✓	91.52	65.36	21.96
VGG-19	✗	90.88	64.86	34.19
VGG-19	✓	91.84	68.79	24.49
AlexNet	✗	79.07	41.41	39.12
DenseNet121	✓	91.97	79.85	34.75
ResNet18	✓	88.65	79.62	31.07

We suspect that the robustness gap due to batch norm for ImageNet is smaller than for other datasets because all models are highly vulnerable by default. We believe this gap could be made larger by training a baseline with greater ℓ_2 regularization (Galloway et al., 2018). For computational reasons, we opt to show this for a simpler dataset in Section 4.

Finally, we explore the role of batch size and depth in Figure 2. Batch norm limits the maximum trainable depth, which *increases* with the batch size, but quickly plateaus as predicted by Theorem 3.10 of Yang et al. (2019). Robustness *decreases* with the batch size for depths that maintain a reasonable test accuracy, at around 25 or fewer layers. This tension between clean accuracy and robustness as a function of the batch size is not observed in unnormalized networks. We show the effect of increasing the number of epochs on these trends in Appendix A.5.

4. Vulnerability and Input Dimension

A recent work (Simon-Gabriel et al., 2018) analyzes adversarial vulnerability of batch-normalized networks at initialization time and conjectures based on a scaling analysis that, under the commonly used He et al. (2015) initialization scheme, adversarial vulnerability scales as $\sim \sqrt{d}$.

They also show in experiments that independence between vulnerability and the input dimension can be approximately recovered through adversarial training by projected gradient descent (PGD) (Mądry et al., 2018), with a modest trade-off of clean accuracy. We show that this can be achieved by simpler means and with little to no trade-off through ℓ_2 weight decay, where the regularization constant λ corrects

[3] For which one of ten random seeds failed to achieve better than chance accuracy on the training set, while others performed as expected. We report the first three successful runs for consistency with the other experiments.

[4] `https://pytorch.org/docs/stable/torchvision/models.html`, `v1.1.0`.

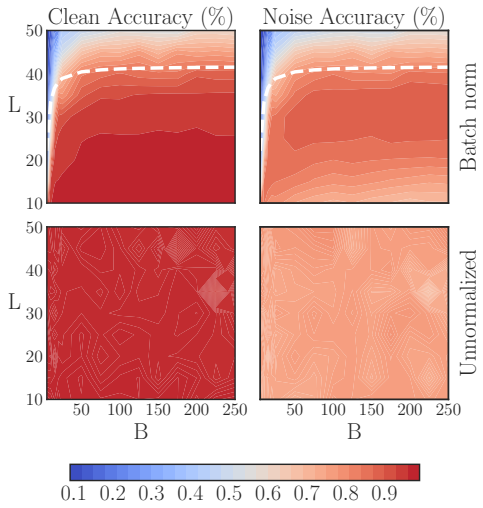

Figure 2. We repeat the experiment of Yang et al. (2019) by training fully-connected nets of depth L and constant-width ReLU layers for ten epochs by SGD, and learning rate $\eta = 10^{-5}B$ for batch size B on MNIST. The batch norm parameters γ and β were left as default, momentum was disabled, and $c = 10^{-3}$. The dashed line is the theoretical maximum trainable depth as a function of batch size. Trials averaged over three random seeds.

the loss scaling as the norm of the input increases with d.

We increase the MNIST image width $\sqrt{d}$ from 28 to 56, 84, and 112 pixels. The loss $\mathcal{L}$ is predicted to grow like $\sqrt{d}$ for ϵ-sized attacks by Thm. 4 of Simon-Gabriel et al. (2018). We confirm that without regularization the loss does scale roughly as predicted: the predicted values lie between loss ratios obtained for $\epsilon = 0.05$ and $\epsilon = 0.1$ attacks for most image widths (see Table 4 of Appendix B). Training with ℓ_2 weight decay, however, we obtain adversarial test accuracy ratios of 0.98 ± 0.01, 0.96 ± 0.04, and 1.00 ± 0.03 and clean accuracy ratios of 0.999 ± 0.002, 0.996 ± 0.003, and 0.987 ± 0.004 for $\sqrt{d}$ of 56, 84, and 112 respectively, relative to the original $\sqrt{d} = 28$ dataset. A more detailed explanation and results are provided in Appendix B.

Next, we repeat this experiment with a two-hidden-layer ReLU MLP, with the number of hidden units equal to the half the input dimension, and optionally use one hidden layer with batch norm.[5] To evaluate robustness, 100 iterations of BIM-ℓ_∞ were used with a step size of 1e-3, and $\epsilon_\infty = 0.1$. We also report test accuracy with additive Gaussian noise of zero mean and unit variance, the same first two moments as the clean images.[6]

[5]This choice of architecture is mostly arbitrary, the trends were the same for constant width layers.

[6]We first apply the noise to the original 28×28 pixel images, then resize them to preserve the appearance of the noise.

Table 6. Evaluating the robustness of a MLP with and without batch norm. We observe a $61 \pm 1\%$ reduction in test accuracy due to batch norm for $\sqrt{d} = 84$ compared to $\sqrt{d} = 28$.

Model		Test Accuracy (%)		
$\sqrt{d}$	BN	Clean	Noise	$\epsilon = 0.1$
28	✗	97.95 ± 0.08	93.0 ± 0.4	66.7 ± 0.9
	✓	97.88 ± 0.09	76.6 ± 0.7	22.9 ± 0.7
56	✗	98.19 ± 0.04	93.8 ± 0.1	53.2 ± 0.7
	✓	98.22 ± 0.02	79.3 ± 0.6	8.6 ± 0.8
84	✗	98.27 ± 0.04	94.3 ± 0.1	47.6 ± 0.8
	✓	98.28 ± 0.05	80.5 ± 0.6	6.1 ± 0.5

Table 7. Evaluating the robustness of a MLP with ℓ_2 weight decay (same λ as for linear model, see Table 11 of Appendix B). Adding batch norm degrades all accuracies.

Model		Test Accuracy (%)		
$\sqrt{d}$	BN	Clean	Noise	$\epsilon = 0.1$
56	✗	97.62 ± 0.06	95.93 ± 0.06	87.9 ± 0.2
	✓	96.23 ± 0.03	90.22 ± 0.18	66.2 ± 0.8
84	✗	96.99 ± 0.05	95.69 ± 0.09	87.9 ± 0.1
	✓	93.30 ± 0.09	87.72 ± 0.11	65.1 ± 0.5

Despite a difference in clean accuracy of only $0.08 \pm 0.05\%$, Table 6 shows that for the original image resolution, batch norm reduced accuracy for noise by $16.4 \pm 0.4\%$, and for BIM-ℓ_∞ by $43.8 \pm 0.5\%$. Robustness keeps decreasing as the image size increases, with the batch-normalized network having $\sim 40\%$ less robustness to BIM and $13 - 16\%$ less to noise at all sizes.

We then apply the ℓ_2 regularization constants tuned for the respective input dimensions on the linear model to the ReLU MLP with no further adjustments. Table 7 shows that by adding sufficient ℓ_2 regularization ($\lambda = 0.01$) to recover the original ($\sqrt{d} = 28$, no BN) accuracy for BIM of $\approx 66\%$ when using batch norm, we induce a test error increase of $1.69 \pm 0.01\%$, which is substantial on MNIST. Furthermore, using the same regularization constant without batch norm increases clean test accuracy by $1.39 \pm 0.04\%$, and for the BIM-ℓ_∞ perturbation by $21.7 \pm 0.4\%$.

Following the guidance in the original work on batch norm (Ioffe & Szegedy, 2015) to the extreme ($\lambda = 0$): to *reduce* weight decay when using batch norm, accuracy for the $\epsilon_\infty = 0.1$ perturbation is degraded by $79.3 \pm 0.3\%$ for $\sqrt{d} = 56$, and $81.2 \pm 0.2\%$ for $\sqrt{d} = 84$. *In all cases, using batch norm greatly reduced test accuracy for noisy and adversarially perturbed inputs, while weight decay increased accuracy for such inputs.*

5. Conclusion

We found that there is no free lunch with batch norm: the accelerated training properties and occasionally higher clean test accuracy come at the cost of robustness, both to additive noise and for adversarial perturbations. We have shown that there is no inherent relationship between the input dimension and vulnerability. Our results highlight the importance of identifying the disparate mechanisms of regularization techniques, especially when concerned about robustness.

Acknowledgements

The authors wish to acknowledge the financial support of NSERC, CFI, CIFAR and EPSRC. We also acknowledge hardware support from NVIDIA and Compute Canada. Research at the Perimeter Institute is supported by Industry Canada and the province of Ontario through the Ministry of Research & Innovation. We thank Thorsteinn Jonsson for helpful discussions; Colin Brennan, Terrance DeVries and Jörn-Henrik Jacobsen for technical suggestions; Justin Gilmer for suggesting the common corruption benchmark; Maeve Kennedy, Vithursan Thangarasa, Katya Kudashkina, and Boris Knyazev for comments and proofreading.

References

Athalye, A., Carlini, N., and Wagner, D. Obfuscated Gradients Give a False Sense of Security: Circumventing Defenses to Adversarial Examples. In *International Conference on Machine Learning*, pp. 274–283, 2018.

Bjorck, N., Gomes, C. P., Selman, B., and Weinberger, K. Q. Understanding Batch Normalization. In *Advances in Neural Information Processing Systems 31*, pp. 7705–7716. Curran Associates, Inc., 2018.

Brendel, W. and Bethge, M. Approximating CNNs with Bag-of-local-Features models works surprisingly well on ImageNet. In *International Conference on Learning Representations*, 2019.

Ding, G. W., Wang, L., and Jin, X. AdverTorch v0.1: An Adversarial Robustness Toolbox based on PyTorch. *arXiv preprint arXiv:1902.07623*, 2019.

Ford, N., Gilmer, J., and Cubuk, E. D. Adversarial Examples Are a Natural Consequence of Test Error in Noise. 2019.

Galloway, A., Tanay, T., and Taylor, G. W. Adversarial Training Versus Weight Decay. *arXiv preprint arXiv:1804.03308*, 2018.

Geirhos, R., Rubisch, P., Michaelis, C., Bethge, M., Wichmann, F. A., and Brendel, W. ImageNet-trained CNNs are biased towards texture; increasing shape bias improves accuracy and robustness. In *International Conference on Learning Representations*, 2019.

Gilmer, J., Metz, L., Faghri, F., Schoenholz, S., Raghu, M., Wattenberg, M., and Goodfellow, I. Adversarial Spheres. In *International Conference on Learning Representations Workshop Track*, 2018.

Goodfellow, I. J., Shlens, J., and Szegedy, C. Explaining and Harnessing Adversarial Examples. In *International Conference on Learning Representations*, 2015.

He, K., Zhang, X., Ren, S., and Sun, J. Delving Deep into Rectifiers: Surpassing Human-Level Performance on ImageNet Classification. In *International Conference on Computer Vision*, pp. 1026–1034. IEEE Computer Society, 2015.

Hendrycks, D. and Dietterich, T. Benchmarking Neural Network Robustness to Common Corruptions and Perturbations. In *International Conference on Learning Representations*, 2019.

Hoffer, E., Hubara, I., and Soudry, D. Train longer, generalize better: Closing the generalization gap in large batch training of neural networks. In *Advances in Neural Information Processing Systems 30*, pp. 1731–1741. Curran Associates, Inc., 2017.

Ioffe, S. and Szegedy, C. Batch normalization: Accelerating deep network training by reducing internal covariate shift. In *International Conference on Machine Learning*, 2015.

Jacobsen, J.-H., Behrmann, J., Carlini, N., Tramèr, F., and Papernot, N. Exploiting Excessive Invariance caused by Norm-Bounded Adversarial Robustness. *Safe Machine Learning workshop at ICLR*, 2019.

Kurakin, A., Goodfellow, I. J., and Bengio, S. Adversarial Machine Learning at Scale. *International Conference on Learning Representations*, 2017.

Mądry, A., Makelov, A., Schmidt, L., Tsipras, D., and Vladu, A. Towards Deep Learning Models Resistant to Adversarial Attacks. In *International Conference on Learning Representations*, 2018.

Recht, B., Roelofs, R., Schmidt, L., and Shankar, V. Do CIFAR-10 Classifiers Generalize to CIFAR-10? *arXiv:1806.00451*, 2018.

Schmidt, L., Santurkar, S., Tsipras, D., Talwar, K., and Mądry, A. Adversarially Robust Generalization Requires More Data. In *Advances in Neural Information Processing Systems 31*, pp. 5014–5026. Curran Associates, Inc., 2018.

Schott, L., Rauber, J., Bethge, M., and Brendel, W. Towards the first adversarially robust neural network model on MNIST. In *International Conference on Learning Representations*, 2019.

Sculley, D., Snoek, J., Wiltschko, A., and Rahimi, A. Winner's Curse? On Pace, Progress, and Empirical Rigor. In *International Conference on Learning Representations, Workshop*, 2018.

Simon-Gabriel, C.-J., Ollivier, Y., Bottou, L., Schölkopf, B., and Lopez-Paz, D. Adversarial Vulnerability of Neural Networks Increases With Input Dimension. *arXiv:1802.01421 [cs, stat]*, 2018.

Soudry, D., Hoffer, E., Nacson, M. S., and Srebro, N. The Implicit Bias of Gradient Descent on Separable Data. In *International Conference on Learning Representations*, 2018.

Su, D., Zhang, H., Chen, H., Yi, J., Chen, P.-Y., and Gao, Y. Is Robustness the Cost of Accuracy? – A Comprehensive Study on the Robustness of 18 Deep Image Classification Models. In *Computer Vision – ECCV 2018*, pp. 644–661. Springer International Publishing, 2018. ISBN 978-3-030-01258-8.

Szegedy, C., Zaremba, W., Sutskever, I., Bruna, J., Erhan, D., Goodfellow, I., and Fergus, R. Intriguing properties of neural networks. In *International Conference on Learning Representations*, 2014.

Tanay, T. and Griffin, L. D. A Boundary Tilting Persepective on the Phenomenon of Adversarial Examples. *arXiv:1608.07690*, 2016.

Tsipras, D., Santurkar, S., Engstrom, L., Turner, A., and Mądry, A.

Robustness May Be at Odds with Accuracy. In *International Conference on Learning Representations*, 2019.

van Laarhoven, T. L2 Regularization versus Batch and Weight Normalization. *arXiv:1706.05350*, 2017.

Yang, G., Pennington, J., Rao, V., Sohl-Dickstein, J., and Schoenholz, S. S. A Mean Field Theory of Batch Normalization. In *International Conference on Learning Representations*, 2019.

Zhang, G., Wang, C., Xu, B., and Grosse, R. Three Mechanisms of Weight Decay Regularization. In *International Conference on Learning Representations*, 2019a.

Zhang, H., Dauphin, Y. N., and Ma, T. Residual Learning Without Normalization via Better Initialization. In *International Conference on Learning Representations*, 2019b.

A. Appendix to Empirical Results

This section contains supplementary explanations and results to those of Section 3.

A.1. Why the VGG Architecture?

For SVHN and CIFAR-10 experiments, we selected the VGG family of models as a simple yet contemporary convolutional architecture whose development occurred independent of batch norm. This makes it suitable for a causal intervention, given that we want to study the effect of batch norm itself, and not batch norm + other architectural innovations + hyperparameter tuning. State-of-the-art architectures such as Inception, and ResNet whose development is more intimately linked with batch norm may be less suitable for this kind of analysis. The superior standard test accuracy of these models is somewhat moot given a trade-off between standard test accuracy and robustness, demonstrated in this work and elsewhere (Tanay & Griffin, 2016; Galloway et al., 2018; Su et al., 2018; Tsipras et al., 2019). Aside from these reasons, and provision of pre-trained variants on ImageNet with and without batch norm in `torchvision.models` for ease of reproducibility, this choice of architecture is arbitrary.

A.2. Comparison of PGD to BIM

We used the PGD implementation from Ding et al. (2019) with settings as below. The pixel range was set to $\{\pm 1\}$ for SVHN, and $\{\pm 2\}$ for CIFAR-10 and ImageNet:

```
from advertorch.attacks import LinfPGDAttack
adversary = LinfPGDAttack(net, loss_fn=nn.CrossEntropyLoss(reduction="sum"),
    eps=0.03, nb_iter=20, eps_iter=0.003,
    rand_init=False, clip_min=-1.0, clip_max=1.0, targeted=False)
```

We compared PGD using a step size of $\epsilon/10$ to our own BIM implemenation with a step size of $\epsilon/20$, for the same number (20) of iterations. This reduces test accuracy for $\epsilon_\infty = 0.03$ perturbations from $31.3 \pm 0.2\%$ for BIM to $27.1 \pm 0.3\%$ for PGD for the unnormalized VGG8 network, and from $15 \pm 1\%$ to $10 \pm 1\%$ for the batch-normalized network. The difference due to batch norm is identical in both cases: $17 \pm 1\%$. Results were also consistent between PGD and BIM for ImageNet. We also tried increasing the number of PGD iterations for deeper networks. For VGG16 on CIFAR-10, using 40 iterations of PGD with a step size of $\epsilon_\infty/20$, instead of 20 iterations with $\epsilon_\infty/10$, reduced accuracy from $28.9 \pm 0.2\%$ to $28.5 \pm 0.3\%$, a difference of only $0.4 \pm 0.5\%$.

A.3. Additional SVHN and CIFAR-10 Results for Deeper Models

Our first attempt to train VGG models on SVHN with more than 8 layers failed, therefore for a fair comparison we report the robustness of the deeper models that were only trainable by using batch norm in Table 8. None of these models obtained much better robustness in terms of PGD-ℓ_2, although they did better for PGD-ℓ_∞.

Table 8. VGG variants on SVHN with batch norm.

	Test Accuracy (%)			
L	Clean	Noise	PGD-ℓ_∞	PGD-ℓ_2
11	95.31 ± 0.03	80.5 ± 1	20.2 ± 0.2	6.1 ± 0.2
13	95.88 ± 0.05	77.2 ± 7	21.7 ± 0.5	5.4 ± 0.2
16	94.59 ± 0.05	78.1 ± 4	19.2 ± 0.3	3.0 ± 0.2
19	95.1 ± 0.3	78 ± 1	24.2 ± 0.6	4.1 ± 0.4

Fixup initialization was recently proposed to reduce the use of normalization layers in deep residual networks (Zhang et al., 2019b). As a natural test we compare a WideResNet (28 layers, width factor 10) with Fixup versus the default architecture with batch norm. Note that the Fixup variant still contains one batch norm layer before the classification layer, but the number of batch norm layers is still greatly reduced.[7]

[7]We used the implementation from `https://github.com/valilenk/fixup`, but stopped training at 150 epochs for consis-

Table 9. Accuracies of WideResNet–28–10 on CIFAR-10 and CIFAR-10.1 (v6).

	CIFAR-10				CIFAR-10.1	
Model	Clean	Noise	PGD-ℓ_∞	PGD-ℓ_2	Clean	Noise
Fixup	94.6 ± 0.1	69.1 ± 1.1	20.3 ± 0.3	9.4 ± 0.2	87.5 ± 0.3	67.8 ± 0.9
BN	95.9 ± 0.1	57.6 ± 1.5	14.9 ± 0.6	8.3 ± 0.3	89.6 ± 0.2	58.3 ± 1.2

We train WideResNets (WRN) with five unique seeds and show their test accuracies in Table 9. Consistent with Recht et al. (2018), higher clean test accuracy on CIFAR-10, i.e. obtained by the WRN compared to VGG, translated to higher clean accuracy on CIFAR-10.1. However, these gains were wiped out by moderate Gaussian noise. VGG8 dramatically outperforms both WideResNet variants subject to noise, achieving 78.9 ± 0.6 vs. 69.1 ± 1.1. Unlike for VGG8, the WRN showed little generalization gap between noisy CIFAR-10 and 10.1 variants: 69.1 ± 1.1 is reasonably compatible with 67.8 ± 0.9, and 57.6 ± 1.5 with 58.3 ± 1.2. The Fixup variant improves accuracy by $11.6 \pm 1.9\%$ for noisy CIFAR-10, $9.5 \pm 1.5\%$ for noisy CIFAR-10.1, $5.4 \pm 0.6\%$ for PGD-ℓ_∞, and $1.1 \pm 0.4\%$ for PGD-ℓ_2.

We believe our work serves as a compelling motivation for Fixup and other techniques that aim to reduce usage of batch normalization. The role of skip-connections should be isolated in future work since absolute values were consistently lower for residual networks.

A.4. ImageNet Black-box Transferability Analysis

Table 10. ImageNet validation accuracy for adversarial examples transfered between VGG variants of various depths, indicated by number, with and without batch norm ("✓", "✗"). All adversarial examples were crafted with BIM-ℓ_∞ using 10 steps and a step size of 5e-3, which is higher than for the white-box analysis to improve transferability. The BIM objective was simply misclassification, i.e., it was not a targeted attack. For efficiency reasons, we select 2048 samples from the validation set. Values along the diagonal in first two columns for Source = Target indicate white-box accuracy.

			Target							
			11		13		16		19	
Acc. Type	Source		✗	✓	✗	✓	✗	✓	✗	✓
Top 1	11	✗	1.2	42.4	37.8	42.9	43.8	49.6	47.9	53.8
		✓	58.8	0.3	58.2	45.0	61.6	54.1	64.4	58.7
Top 5	11	✗	11.9	80.4	75.9	80.9	80.3	83.3	81.6	85.1
		✓	87.9	6.8	86.7	83.7	89.0	85.7	90.4	88.1

The discrepancy between the results in additive noise and for white-box BIM perturbations for ImageNet in Section 3 raises a natural question: Is *gradient masking* a factor influencing the success of the white-box results on ImageNet? No, consistent with the white-box results, when the target is unnormalized but the source is, top 1 accuracy is $10.5\% - 16.4\%$ higher, while top 5 accuracy is $5.3\% - 7.5\%$ higher, than vice versa. This can be observed in Table 10 by comparing the diagonals from lower left to upper right. When targeting an unnormalized model, we reduce top 1 accuracy by $16.5\% - 20.4\%$ using a source that is also unnormalized, compared to a difference of only $2.1\% - 4.9\%$ by matching batch normalized networks. This suggests that the features used by unnormalized networks are more stable than those of batch normalized networks.

Unfortunately, the pre-trained ImageNet models provided by the PyTorch developers do not include hyperparameter settings or other training details. However, we believe that this speaks to the generality of the results, i.e., that they are not sensitive to hyperparameters.

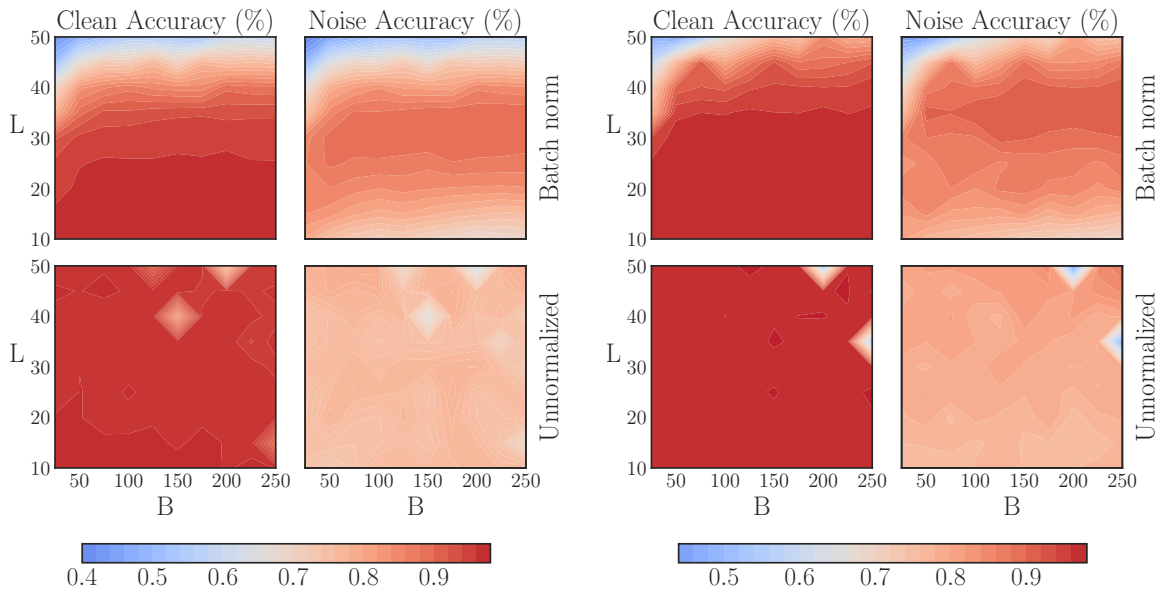

(a) (b)

Figure 3. We repeat the experiment of Yang et al. (2019) by training fully-connected models of depth L and constant width (N_l=384) with ReLU units by SGD, and learning rate $\eta = 10^{-5}B$ for batch size B on MNIST. We train for 10 and 40 epochs in (a) and (b) respectively. The batch norm parameters γ and β were left as default, momentum disabled, and c = 1e-3. Each coordinate is first averaged over three seeds. Diamond shaped artefacts for unnormalized case indicate one of three seeds failed to train – note that we show an equivalent version of (a) with these outliers removed and additional batch sizes from 5–20 in Figure 2. Best viewed in colour.

A.5. Batch Norm Limits Maximum Trainable Depth and Robustness

In Figure 3 we show that batch norm not only limits the maximum trainable depth, but robustness decreases with the batch size for depths that maintain test accuracy, at around 25 or fewer layers (in Figure 3(a)). Both clean accuracy and robustness showed little to no relationship with depth nor batch size in unnormalized networks. A few outliers are observed for unnormalized networks at large depths and batch size, which could be due to the reduced number of parameter update steps that result from a higher batch size and fixed number of epochs (Hoffer et al., 2017).

Note that in Figure 3(a) the bottom row—without batch norm—appears lighter than the equivalent plot above, with batch norm, indicating that unnormalized networks obtain less absolute peak accuracy than the batch normalized network. Given that the unnormalized networks take longer to converge, we prolong training for 40 total epochs. When they do converge, we see more configurations that achieve higher clean test accuracy than batch normalized networks in Figure 3(b). Furthermore, good robustness can be experienced simultaneously with good clean test accuracy in unnormalized networks, whereas the regimes of good clean accuracy and robustness are still mostly non-overlapping in Figure 3(b).

B. Weight Decay and Input Dimension

Consider a logistic regression model with input $x \in \mathbb{R}^d$, labels $y \in \{\pm 1\}$, parameterized by weights w, and bias b. Predictions are defined by $o = w^\top x + b$ and the model can be optimized by stochastic gradient descent (SGD) on the sigmoid cross entropy loss, which reduces to SGD on (2), where ζ is the softplus loss $\zeta(z) = \log(1 + e^{-z})$:

$$\mathbb{E}_{x,y\sim p_{\text{data}}}\, \zeta(y(w^\top x + b)). \tag{2}$$

We note that $w^\top x + b$ is a *scaled*, signed distance between x and the classification boundary defined by our model. If we define $d(x)$ as the signed Euclidean distance between x and the boundary, then we have: $w^\top x + b = \|w\|_2\, d(x)$. Hence,

tency with the VGG8 experiment. Both models had already fit the training set by this point.

minimizing (2) is equivalent to minimizing

$$\mathbb{E}_{x,y\sim p_{\text{data}}}\ \zeta(\|w\|_2 \times y\, d(x)). \tag{3}$$

We define the *scaled softplus loss* as

$$\zeta_{\|w\|_2}(z) := \zeta(\|w\|_2 \times z) \tag{4}$$

and note that adding a ℓ_2 regularization term in (3), resulting in (5), can be understood as a way of controlling the scaling of the softplus function:

$$\mathbb{E}_{x,y\sim p_{\text{data}}}\ \zeta_{\|w\|_2}(y\, d(x)) + \lambda\|w\|_2 \tag{5}$$

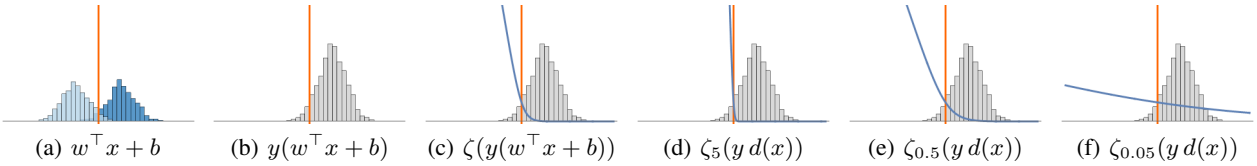

(a) $w^\top x + b$ (b) $y(w^\top x + b)$ (c) $\zeta(y(w^\top x + b))$ (d) $\zeta_5(y\, d(x))$ (e) $\zeta_{0.5}(y\, d(x))$ (f) $\zeta_{0.05}(y\, d(x))$

Figure 4. (a) For a given weight vector w and bias b, the values of $w^\top x + b$ over the training set typically follow a bimodal distribution (corresponding to the two classes) centered on the classification boundary. (b) Multiplying by the label y allows us to distinguish the correctly classified data in the positive region from misclassified data in the negative region. (c) We can then attribute a penalty to each training point by applying the softplus loss to $y(w^\top x + b)$. (d) For a small regularization parameter (large $\|w\|_2$), the misclassified data is penalized linearly while the correctly classified data is not penalized. (e) A medium regularization parameter (medium $\|w\|_2$) corresponds to smoothly blending the margin. (f) For a large regularization parameter (small $\|w\|_2$), all data points are penalized almost linearly.

In Figures 4(a)-4(c), we develop intuition for the different quantities contained in (2) with respect to a typical binary classification problem, while Figures 4(d)-4(f) depict the effect of the regularization parameter λ on the scaling of the loss function.

To test this theory empirically we study a single linear layer on variants of MNIST of increasing input dimension, where the "core idea" from (Simon-Gabriel et al., 2018) is exact. Clearly, this model is too simple to obtain competitive test accuracy, but this is a helpful first step that will be subsequently extended to ReLU networks. The model was trained by SGD for 50 epochs with a constant learning rate of 1e-2 and a batch size of 128. In Table 11 we show that increasing the input dimension by resizing MNIST from 28×28 to various resolutions with `PIL.Image.NEAREST` interpolation increases adversarial vulnerability in terms of accuracy and loss. Furthermore, the "adversarial damage", which is predicted to grow like $\sqrt{d}$ by Theorem 4 of Simon-Gabriel et al. (2018), falls in between that obtained empirically for $\epsilon = 0.05$ and $\epsilon = 0.1$ for all image widths except for 112, which experiences slightly more damage than anticipated.

Simon-Gabriel et al. (2018) note that independence between vulnerability and the input dimension can be recovered through adversarial example augmented training by projected gradient descent (PGD), with a small trade-off in terms of standard test accuracy. We find that the same can be achieved through a much simpler approach: ℓ_2 weight decay, with λ chosen to correct for the loss scaling. This way we recover input dimension invariant vulnerability with little degradation of test accuracy, e.g., see the $\epsilon = 0.1$ accuracy ratio of 1.00 ± 0.03 with ℓ_2 for $\sqrt{d} = 112$ in Table 11 compared to 0.10 ± 0.09 without.

Compared to PGD training, weight decay regularization i) does not have an arbitrary ϵ hyperparameter that ignores inter-sample distances, ii) does not prolong training by a multiplicative factor given by the number of steps in the inner loop, and 3) is less attack-specific. Thus, we do not use adversarially augmented training because we wish to convey a notion of robustness to unseen attacks and common corruptions. Furthermore, enforcing robustness to ϵ-perturbations may increase vulnerability to *invariance-based* examples, where semantic changes are made to the input thus changing the Oracle label, but not the classifier's prediction (Jacobsen et al., 2019). Our models trained with weight decay obtained 12% higher accuracy (86 vs. 74 correct) compared to batch norm on a small sample of 100 ℓ_∞ invariance-based MNIST examples.[8] We make primary use of traditional ℓ_p perturbations as they are well studied in the literature and straightforward to compute, but solely defending against these is not the end goal.

[8]Invariance based adversarial examples downloaded from `https://github.com/ftramer/Excessive-Invariance`.

Table 11. Mitigating the effect of the input dimension on adversarial vulnerability by correcting the margin enforced by the loss function. Regularization constant λ is for ℓ_2 weight decay. Consistent with Simon-Gabriel et al. (2018), we use ϵ-FGSM perturbations, the optimal ℓ_∞ attack for a linear model. Values in rows with $\sqrt{d} > 28$ are ratios of entry (accuracy or loss) wrt the $\sqrt{d} = 28$ baseline. "Pred." is the predicted increase of the loss $\mathcal{L}$ due to a small ϵ-perturbation using Thm. 4 of Simon-Gabriel et al..

Model		Relative Test Accuracy (%)		Relative Loss			
$\sqrt{d}$	λ	Clean	$\epsilon = 0.1$	Clean	$\epsilon = 0.05$	$\epsilon = 0.1$	Pred.
28	–	$92.4 \pm 0.1\%$	$53.9 \pm 0.3\%$	0.268 ± 0.001	0.646 ± 0.001	1.410 ± 0.004	-
56	–	1.001 ± 0.001	0.33 ± 0.03	1.011 ± 0.007	1.802 ± 0.006	2.449 ± 0.009	2
56	0.01	0.999 ± 0.002	0.98 ± 0.01	1.010 ± 0.007	1.010 ± 0.006	1.01 ± 0.01	-
84	–	0.998 ± 0.002	0.10 ± 0.09	1.06 ± 0.01	2.84 ± 0.02	4.15 ± 0.02	3
84	0.0225	0.996 ± 0.003	0.96 ± 0.04	1.05 ± 0.02	1.06 ± 0.03	1.06 ± 0.03	-
112	–	0.992 ± 0.004	0.1 ± 0.2	1.18 ± 0.03	4.15 ± 0.02	5.96 ± 0.02	4
112	0.05	0.987 ± 0.004	1.00 ± 0.03	1.14 ± 0.04	1.08 ± 0.03	1.04 ± 0.03	-

Table 12. Two-hidden-layer ReLU MLP, with and without batch norm (BN), trained for 50 epochs and repeated over five random seeds. Values in rows with $\sqrt{d} > 28$ are ratios wrt the $\sqrt{d} = 28$ baseline (accuracy or loss). There is a considerable increase of the loss, or similarly, a degradation of robustness in terms of accuracy, due to batch norm. The discrepancy for BIM-ℓ_∞ with $\epsilon = 0.1$ for $\sqrt{d} = 84$ with batch norm represents a $61 \pm 1\%$ degradation in absolute accuracy compared to the baseline.

Model		Relative Test Accuracy (%)			Relative Loss		
$\sqrt{d}$	BN	Clean	Noise	$\epsilon = 0.1$	Clean	$\epsilon = 0.05$	$\epsilon = 0.1$
28	✗	97.95 ± 0.08	93.0 ± 0.4	66.7 ± 0.9	0.0669 ± 0.0008	0.285 ± 0.003	1.06 ± 0.02
28	✓	0.9992 ± 0.0012	0.82 ± 0.01	0.34 ± 0.03	1.06 ± 0.04	2.20 ± 0.03	3.18 ± 0.03
56	✗	1.0025 ± 0.0009	1.009 ± 0.004	0.80 ± 0.02	0.87 ± 0.02	1.27 ± 0.01	1.68 ± 0.03
56	✓	1.0027 ± 0.0008	0.853 ± 0.008	0.13 ± 0.09	0.91 ± 0.03	3.48 ± 0.02	5.83 ± 0.03
84	✗	1.0033 ± 0.0009	1.015 ± 0.004	0.71 ± 0.02	0.86 ± 0.02	1.48 ± 0.02	2.15 ± 0.03
84	✓	1.0033 ± 0.0010	0.865 ± 0.009	0.09 ± 0.08	0.88 ± 0.02	4.34 ± 0.02	7.34 ± 0.02

A more detailed comparison between adversarial training and weight decay can be found in Galloway et al. (2018). The scaling of the loss function mechanism of weight decay is complementary to other mechanisms identified in the literature recently, for instance that it also increases the effective learning rate (van Laarhoven, 2017; Zhang et al., 2019a). Our results are consistent with these works in that weight decay reduces the generalization gap, even in batch-normalized networks where it is presumed to have no effect. Given that batch norm is not typically used on the last layer, the loss scaling mechanism persists in this setting although to a lesser degree.

C. Common Corruption Robustness

We evaluated robustness on the common corruptions and perturbations benchmarks (Hendrycks & Dietterich, 2019). Common corruptions are 19 types of real-world effects that can be grouped into four categories: "noise", "blur", "weather", and "digital". Each corruption has five "severity" or intensity levels. These are applied to the test sets of CIFAR-10 and ImageNet, denoted CIFAR-10-C and ImageNet-C respectively. When reporting the mean corruption error (mCE), we average over intensity levels for each corruption, then over all corruptions. We outline the results for two VGG variants and a WideResNet on CIFAR-10-C, trained from scratch independently over three and five random seeds, respectively. The most important results are also summarized in Table 13.

For VGG8 batch norm increased the error rate for all noise variants, at every intensity level. The mean generalization gaps

Table 13. Robustness of three modern convolutional neural network architectures with and without batch norm on the `CIFAR-10-C` common corruptions benchmark (Hendrycks & Dietterich, 2019). We use "F" to denote Fixup (Zhang et al., 2019b), as this variant still had one batch-norm layer. Values were averaged over five intensity levels for each corruption. We report the top five of 19 corruptions by magnitude of the accuracy gap due to batch norm; see the text for more detail on the corruptions omitted here.

Model		Test Accuracy (%)					
Variant	BN	Clean	Gaussian	Impulse	Shot	Speckle	Contrast
VGG8	✗	87.9 ± 0.1	$\mathbf{65.6 \pm 1.2}$	$\mathbf{58.8 \pm 0.8}$	$\mathbf{71.0 \pm 1.2}$	$\mathbf{70.8 \pm 1.2}$	$\mathbf{59.3 \pm 0.8}$
	✓	88.7 ± 0.1	56.4 ± 1.5	51.2 ± 0.1	65.4 ± 1.1	66.3 ± 1.1	54.9 ± 1.0
VGG13	✗	91.74 ± 0.02	$\mathbf{64.5 \pm 0.8}$	$\mathbf{63.3 \pm 0.3}$	$\mathbf{70.9 \pm 0.4}$	$\mathbf{71.5 \pm 0.5}$	65.3 ± 0.6
	✓	93.0 ± 0.1	43.6 ± 1.2	49.7 ± 0.5	56.8 ± 0.9	60.4 ± 0.7	$\mathbf{67.7 \pm 0.5}$
WRN–28–10	F	94.6 ± 0.1	$\mathbf{63.3 \pm 0.9}$	$\mathbf{66.7 \pm 0.9}$	$\mathbf{71.7 \pm 0.7}$	$\mathbf{73.5 \pm 0.6}$	81.2 ± 0.7
	✓	95.9 ± 0.1	51.2 ± 2.7	56.0 ± 2.7	63.0 ± 2.5	66.6 ± 2.5	$\mathbf{86.0 \pm 0.9}$

for noise were: Gaussian—$9.2 \pm 1.9\%$, Impulse—$7.5 \pm 0.8\%$, Shot—$5.6 \pm 1.6\%$, and Speckle—$4.5 \pm 1.6\%$. The next most impactful corruptions were: Contrast—$4.4 \pm 1.3\%$, Spatter—$2.4 \pm 0.7\%$, JPEG—$2.0 \pm 0.4\%$, and Pixelate—$1.3 \pm 0.5\%$. Results for the remaining corruptions were a coin toss as to whether batch norm improved or degraded robustness, as the random error was in the same ballpark as the difference being measured. These were: Weather—Brightness, Frost, Snow, and Saturate; Blur—Defocus, Gaussian, Glass, Zoom and Motion; and Elastic transformation. Averaging over all corruptions we get an mCE gap of $1.9 \pm 0.9\%$ due to batch norm, or a loss of accuracy from $72.9 \pm 0.7\%$ to $71.0 \pm 0.6\%$.

VGG13 results were mostly consistent with VGG8: batch norm increased the error rate for all noise variants, at every intensity level. Particularly notable, the generalization gap enlarged to $26 - 28\%$ for Gaussian noise at severity levels 3, 4, and 5; and $17\%+$ for Impulse noise at levels 4 and 5. Averaging over all levels, we have gaps for noise variants of: Gaussian—$20.9 \pm 1.4\%$, Impulse—$13.6 \pm 0.6\%$, Shot—$14.1 \pm 1.0\%$, and Speckle—$11.1 \pm 0.8\%$. Robustness to the other corruptions seemed to benefit from the slightly higher clean test accuracy of $1.3 \pm 0.1\%$ due to batch norm for VGG13. The remaining generalization gaps varied from (negative) $0.2 \pm 1.3\%$ for Zoom blur, to $2.9 \pm 0.6\%$ for Pixelate. Overall mCE was reduced by $2.0 \pm 0.3\%$ for the unnormalized network.

For a WideResNet 28–10 (WRN) using "Fixup" initialization (Zhang et al., 2019b) to reduce the use of batch norm, the mCE was similarly reduced by $1.6 \pm 0.4\%$. Unpacking each category, the mean generalization gaps for noise were: Gaussian—$12.1 \pm 2.8\%$, Impulse—$10.7 \pm 2.9\%$, Shot—$8.7 \pm 2.6\%$, and Speckle—$6.9 \pm 2.6\%$. Note that the large uncertainty for these measurements is due to high variance for the model with batch norm, on average 2.3% versus 0.7% for Fixup. JPEG compression was next at $4.6 \pm 0.3\%$.

Interestingly, some corruptions that led to a positive gap for VGG8 showed a negative gap for the WRN, i.e., batch norm improved accuracy to: Contrast—$4.9 \pm 1.1\%$, Snow—$2.8 \pm 0.4\%$, Spatter—$2.3 \pm 0.8\%$. These were the same corruptions for which VGG13 lost, or did not improve its robustness when batch norm was removed, hence why we believe these correlate with standard test accuracy (highest for WRN). Visually, these corruptions appear to preserve texture information. Conversely, noise is applied in a spatially global way that disproportionately degrades these textures, emphasizing shapes and edges. It is now well known that modern CNNs trained on standard datasets have a propensity to rely excessively on texture rather than shape cues (Geirhos et al., 2019; Brendel & Bethge, 2019). The WRN obtains ≈ 0 training error and is in our view over-fitted; CIFAR-10 is known to be difficult to learn robustly given few samples (Schmidt et al., 2018).

D. Adversarial Spheres

The "Adversarial Spheres" dataset contains points sampled uniformly from the surfaces of two concentric n-dimensional spheres with radii $R = 1$ and $R = 1.3$ respectively, and the classification task is to attribute a given point to the inner or outer sphere. We consider the case $n = 2$, that is, datapoints from two concentric circles. This simple problem poses a challenge to the conventional wisdom regarding batch norm: not only does batch norm harm robustness, it makes training less stable. In Figure 6 we show that, using the same architecture as in Gilmer et al. (2018), the batch-normalized network is highly sensitive to the learning rate η. We use SGD instead of Adam to avoid introducing unnecessary complexity, and especially since SGD has been shown to converge to the maximum-margin solution for linearly separable data (Soudry et al.,

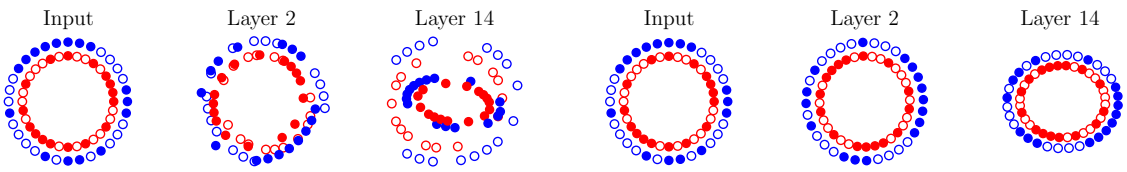

(a) (b)

Figure 5. Two mini-batches from the "Adversarial Spheres" dataset (2D variant), and their representations in a deep linear network at initialization time (a) with batch norm and (b) without batch norm. Mini-batch membership is indicated by marker fill and class membership by colour. Each layer is projected to its two principal components. In (b) we scale both components by a factor of 100, as the dynamic range decreases with depth under default initialization. We observe in (a) that some samples are already overlapping at Layer 2, and classes are mixed at Layer 14.

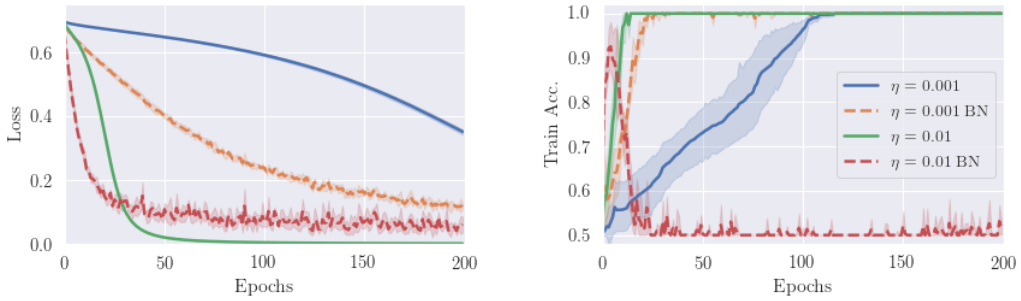

(a) (b)

Figure 6. We train the same two-hidden-layer fully connected network of width 1000 units using ReLU activations and a mini-batch size of 50 on a 2D variant of the "Adversarial Spheres" binary classification problem (Gilmer et al., 2018). Dashed lines denote the model with batch norm. The batch-normalized model fails to train for a learning rate of $\eta = 0.01$, which otherwise converges quickly for the unnormalized equivalent. We repeat the experiment over five random seeds, shaded regions indicate a 95% confidence interval.

2018). We use a finite dataset of 500 samples from $\mathcal{N}(0, I)$ projected onto the circles. The unormalized network achieves zero training error for η up to 0.1 (not shown), whereas the batch-normalized network is already untrainable at $\eta = 0.01$. To evaluate robustness, we sample 10,000 test points from the same distribution for each class (20k total), and apply noise drawn from $\mathcal{N}(0, 0.005 \times I)$. We evaluate only the models that could be trained to 100% training accuracy with the smaller learning rate of $\eta = 0.001$. The model with batch norm classifies 94.83% of these points correctly, while the unnormalized net obtains 96.06%.

E. Qualitative Effect of Batch Normalization

We show a qualitative aspect of batch norm by visualizing the activations of the penultimate hidden layer in a fully-connected network (a) without and (b) with batch norm over the course of 500 epochs. In the unnormalized network 7(a), all data points are overlapping at initialization. Over the first ≈ 20 epochs, the points spread further apart (middle plot) and begin to form clusters. In the final stage (epochs $\approx 300 - 500$), the clusters become tighter. When we introduce two batch-norm layers in the network, placing them before the visualized layer, the activation patterns display notable differences, as shown in Figure 7(b): i) at initialization, all data points are spread out, allowing easier partitioning into clusters and thus facilitating faster training; ii) the clusters are more stationary, and the stages of cluster formation and tightening are not as strictly separated; iii) the inter-cluster distance and the clusters themselves are larger, indicating that the decision boundary is more sensitive to small input variations.

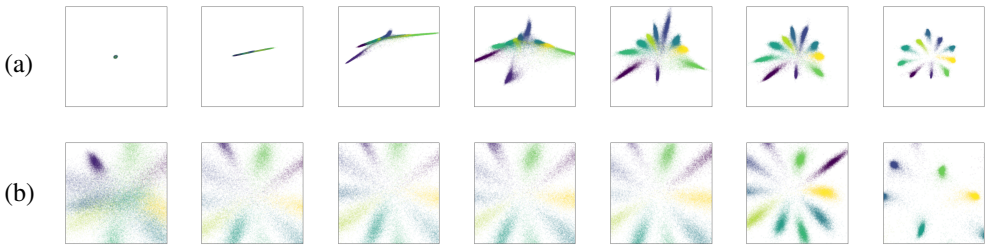

Figure 7. Visualization of activations in a two-unit layer over 500 epochs. Architecture is a fully-connected MLP [(a) (784–392–196–2–49–10) and (b) (784–392–BN–196–BN–2–49–10)] with ReLU units, mini-batch size 128, constant learning rate 1e-2, and weight decay λ=1e-3. The plots have a fixed x- and y-axis range of ± 10. Plotted are all samples from the MNIST training set, colour-coded by label.

F. Author Contributions

In the spirit of Sculley et al. (2018), we provide a summary of each author's contributions.

- First author formulated the hypothesis, conducted the experiments, and wrote the initial draft.
- Second author prepared detailed technical notes on the main references, met frequently with the first author to advance the work, and critically revised the manuscript.
- Third author originally conceived the key theoretical concept of Appendix B as well as some of the figures, and provided important technical suggestions and feedback.
- Fourth author met with the first author to discuss the work and helped revise the manuscript.
- Senior author critically revised several iterations of the manuscript, helped improve the presentation, recommended additional experiments, and sought outside feedback.